NASA
Technical
Memorandum

NASA TM - 108416

EVALUATION OF CHEMICAL CONVERSION MATERIAL (PROTECTIVE COATING) EXPOSED TO SPACE ENVIRONMENTAL CONDITIONS
CDDF Final Report (No. 90-07)

By D.L. Edwards

Materials and Processes Laboratory
Science and Engineering Directorate

July 1993

National Aeronautics and
Space Administration

George C. Marshall Space Flight Center

TABLE OF CONTENTS

LIST OF ILLUSTRATIONS

TECHNICAL MEMORANDUM

EVALUATION OF CHEMICAL CONVERSION MATERIAL (PROTECTIVE COATING) EXPOSED TO SPACE ENVIRONMENTAL CONDITIONS

INTRODUCTION

The space environment has historically been detrimental to materials functioning in space. Numerous examples of this detriment have been observed on the Long Duration Exposure Facility (LDEF).[1] A material present on the LDEF and integral to many other space structures is anodized coatings. The anodize layer is tailored to provide maximum reflectance over a range of wavelengths. A decrease in reflectance of the anodize coating due to space environmental exposure is a primary concern. The space environment contains atomic oxygen (AO), ultraviolet (UV) radiation, high vacuum, meteoroid and debris (M/D), and charged particle radiation. This report focuses on the effect of charged particle irradiation on anodized coatings.

The charged particle environment consists mainly of solar cosmic rays, magnetically trapped protons and electrons, and galactic cosmic rays.[2] These particles range in energy from electron volts (eV) to giga electron volts (GeV). The number density of particles varies with energy and generally decreases with increasing particle energy.

This investigation utilized the test systems within the Space Environmental Effects Facility (SEEF). Prior to this investigation, modification of the Van de Graaff facility was completed. This modified facility is the combined environmental effects test cell 2 (CEETC2) and will be discussed in the description section of this report. The systems operating in the SEEF are capable of providing protons and electrons over the energy range from 100 KeV to 2.5 MeV.

This report focuses on the development of an operational Rutherford backscattering spectrometry (RBS) system and shows the application of such a system on a space environmental effects test.

RBS has the unique capability to obtain depth profiling information during a nondestructive test. Utilization of RBS to examine the metal/metal oxide interface will be demonstrated with the specified task of determining the existence of radiation enhanced diffusion (RED).

Total hemispherical reflectance techniques were used to measure the change in reflectance of the anodized surface as a function of wavelength. The instrument used to measure the change in reflectance was a laboratory portable spectroreflectometer (LPSR). The theory and operation of this instrument are described in reference 3.

DESCRIPTION OF THE FACILITY

Before any exposures could be initiated, the Van de Graaff system required a configuration modification. The 2.5-MeV Van de Graaff required an internal configuration change from electron to proton generation. Justification for conversion to proton generation mode was to incorporate the RBS analytical capability. The RBS technique will be discussed in the analytical theory section of this report.

A beam transport system, which allows the beam to propagate from the accelerator to the test chamber, was configured and operates at a nominal pressure of 2×10^{6} torr. Figure 1 diagrams the CEETC2 system. The transport system contains a beam profile monitor (BPM), which measures the cross-sectional area and position of the proton beam and a Faraday cup to measure the proton beam current. An analyzing magnet is included in the transport system to mass analyze the proton beam. A raster scanner was incorporated in the transport system to provide uniform distribution of charge across the sample surface. The raster scanner provides 97-percent uniform distribution of charge across a maximum surface area of 6 by 6 in.

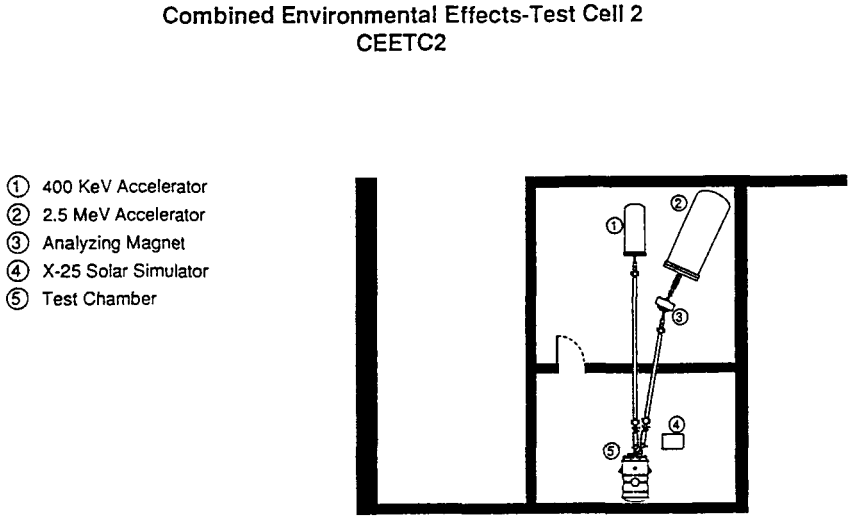

Figure 1. Diagram of the CEETC2 system.

A sample holder was designed which will allow samples to be exposed to a uniform distribution of charge and which has the correct geometrical configuration to allow RBS analysis subsequent to exposure. Figure 2 shows the multisample holder designed for RBS analysis.

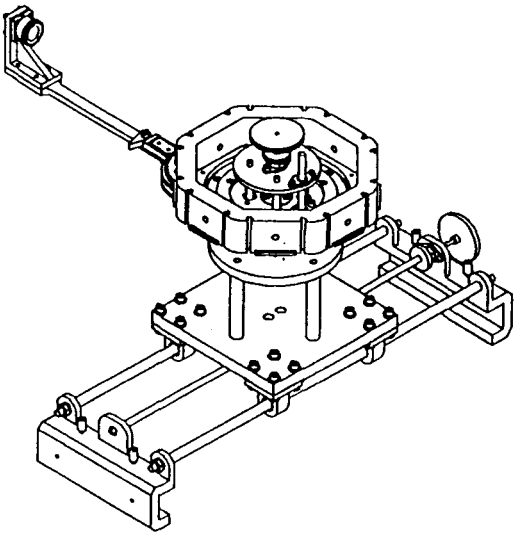

Figure 2. Multisample RBS sample holder used in the CEETC2 system.

DESCRIPTION OF THE TECHNIQUE

Anodization

Techniques have been developed and used to anodize thin films of aluminum (Al) and tantalum (Ta) on thick carbon (diamond) substrates. Four samples (two Al and two Ta) have been anodized and characterized using RBS and total hemispherical reflectance. Figure 3 shows the preexposure RBS spectra of the anodized Al and Ta samples. Figure 4 shows the preexposure reflectance spectra for these samples. The techniques for Al and Ta anodization are described in the following.

Tantalum

Samples consisting of approximately 4,000 Å on thick C (diamond) substrates were prepared by electron beam deposition. These thin films were anodized following procedures outlined in reference 4.

The anodizing solution was 0.035 mole/liter Na_2-SO_4. No special cleaning procedures other than acetone, methanol, and distilled H_2-O rinses (each 1 min in duration) were used prior to immersion in the Na_2-SO_4. Typical parameters for a Ta sample were:

Ta film: 4 mm by 4 mm by 4,000 Å

Time: 60 min

Voltage: 80 V

Current: 250 to 390 mA

Anode-cathode separation: ≈5 cm.

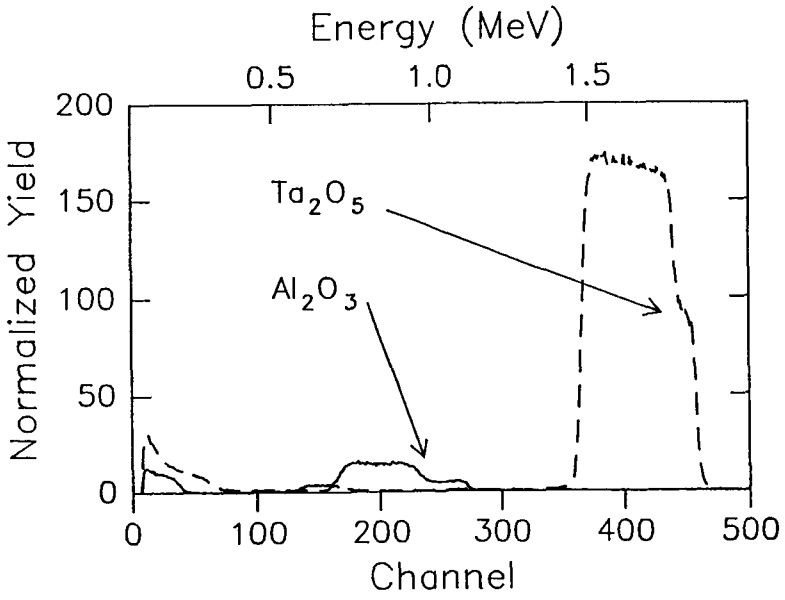

Figure 3. Preexposure RBS spectra of anodized Al and anodized Ta.

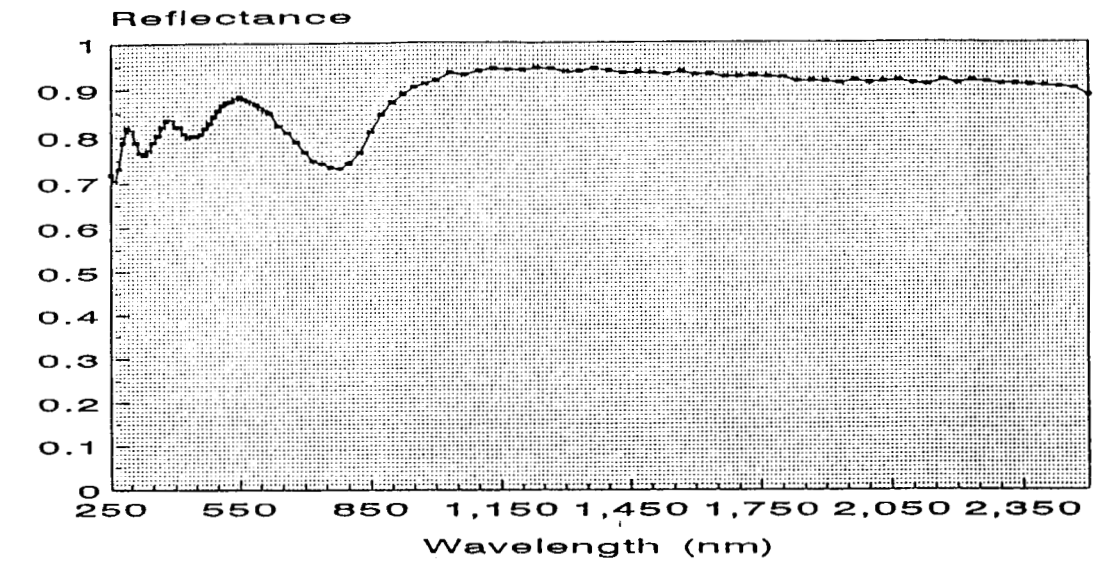

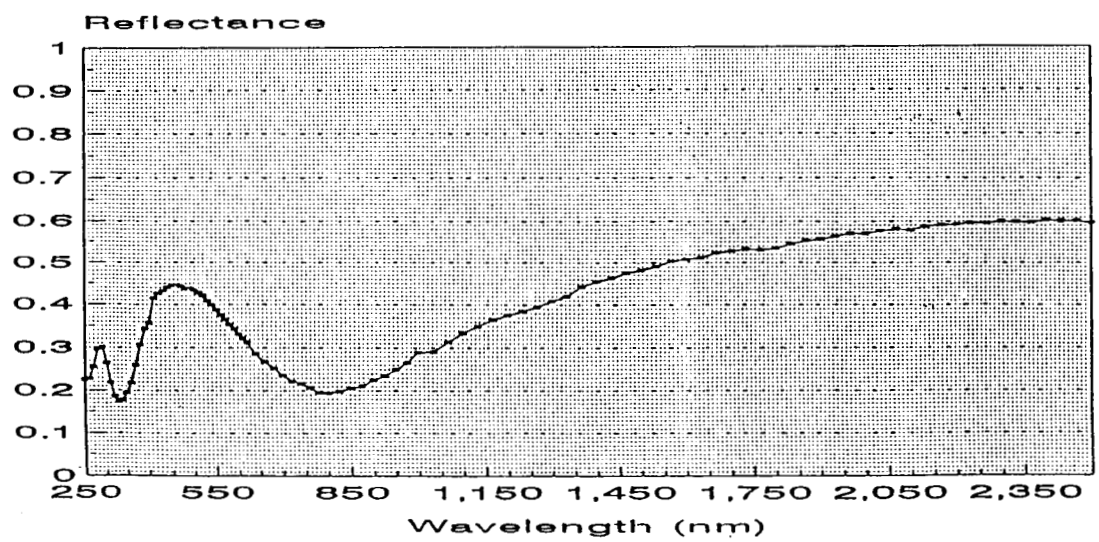

Figure 4. Preexposure reflectance spectra of anodized Al and anodized Ta.

Aluminum

Aluminum proved to be a difficult metal to anodize consistently with oxide layers of more than 100 or 200 Å. Several methods were attempted, and all involved the experimental arrangement of figure 5. Success in anodizing Al came using procedures described in reference 5. Typical parameters were the following:

- Room temperature solution of 2.1M H_2-SO_4
- Pt cathode, Au anode at 5-cm separation
- 1.5 to 2.5 V, 3 to 4 mA for 10 to 15 min
- O_2 saturation via bubbling.

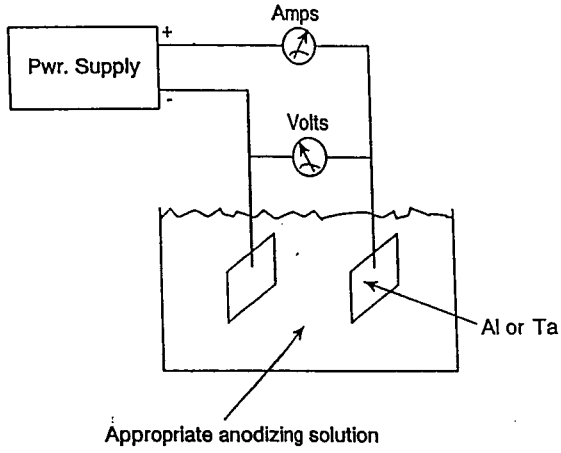

Figure 5. Experimental arrangement used to anodize the Al and Ta samples.

Procedure

Once the samples were anodized, control data were accumulated using RBS and total hemispherical reflectance. The samples were exposed to proton radiation according to the exposure sequence shown in table 1.

Table 1. Radiation exposure sequence for the anodized Al and anodized Ta samples.

Anodized Sample	Energy	Flux (protons/cm^2*s)	Fluence (protons/cm^2)
Aluminum	0.5 MeV	4.83 E10	1.01 E15
Tantalum	0.5 MeV	4.83 E10	1.01 E15
Aluminum	2.0 MeV	4.90 E10	1.01 E15
Tantalum	2.0 MeV	4.90 E10	1.01 E15

Postexposure analysis consisted of total hemispherical reflectance measurements and RBS.

Analytical Theory

RBS is based on the concepts of coulomb scattering and heavy ion energy loss in matter, and in most applications, the heavy ions used in RBS analysis are alpha particles. A collimated beam of mono-energetic alpha particles impinges on a target, and a small fraction of these particles are scattered due to coulombic interactions with atomic nuclei in the target.

Scattering may occur at the front surface of the target or at depths within the target. If the alpha particle does not scatter from the surface but rather penetrates the target, the alpha particle loses energy continuously during the penetration due to coulomb interactions with atomic electrons. For particles with energies of several MeV, the energy loss per unit path length increases with decreasing particle energy. This energy loss process for the penetrating alpha particle yields information related to the depth within a sample at which a scattering event takes place.

An RBS spectrum is a two-dimensional plot which consists of the measured energy of the back-scattered alpha particles on the abscissa and the number of backscattered particles (counts) detected per unit energy as the ordinate. The kinematic factor K governs the energy axis (abscissa) and is given by[6]

$$K = \left\{\left[\left(M_2^2 - M_1^2 \sin^2\theta\right)^{1/2} + M_1 \cos\theta\right] / \left[M_2 + M_1\right]\right\}^2 . \qquad (1)$$

The kinematic factor depends only upon the mass of the incident particle M_1, the mass of the target particle M_2, and the angle through which the incident particles are scattered, θ (fig. 6). Equation (1) is derived through application of the principles of conservation of energy and linear momentum.

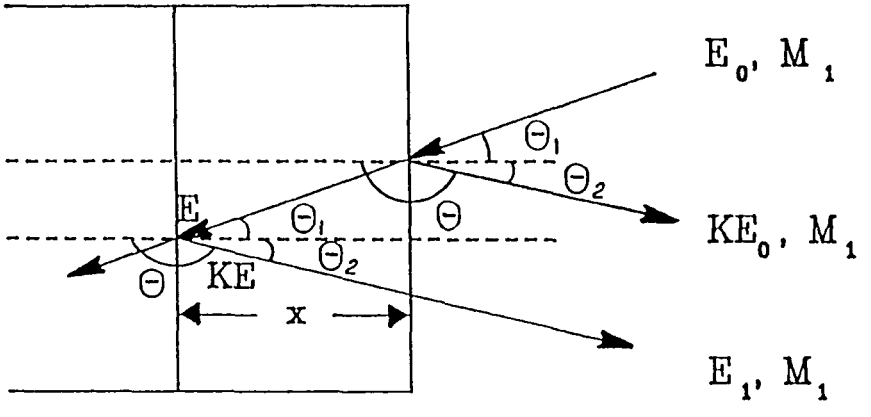

Figure 6. Cross-sectional view of backscattering events in a sample.

The Rutherford scattering cross section, $d\sigma/d\Omega$ (or σ) governs the yield axis (ordinate) and is given by[6]

$$\sigma = \left[Z_1 Z_2 e^2/4E\right]^2 * \left[4/\sin^4\theta\right] * \left\{\left[1 - ((M_{12})\sin\theta)^2\right]^{1/2} + \cos\theta\right\}^2 * 1/\left[1 - ((M_{12})\sin\theta)^2\right]^{1/2} . \qquad (2)$$

The variable M_{12} is defined as the ratio (M_1/M_2). The scattering cross section varies directly with the square of the atomic number, Z_2, of the target nucleus. As a result, equal concentrations of light and heavy target nuclei produce different yields in an RBS spectrum.

The energy distribution of the backscattered alpha particle provides depth profiling information. The transformation from measured energy to depth is accomplished through consideration of the alpha particle energy loss per unit path length dE/dx. As an incident particle penetrates the sample, it slows down, and the kinetic energy of the incident particle decreases. The magnitude of the energy loss per unit length depends upon the identity of the incident particle and the density and composition of the target atoms. Scattering events which occur at the front surface of the target layer produce particles with energy

$$E_i = KE_0 \ , \tag{3}$$

where E_0 is the energy of the incident particle. E_i is the highest energy a backscattered particle may have.

Once the incident particle has penetrated the target, the energy loss process must be considered along the inward path of the incident particle and along the outward path of the scattered particle. In figure 6, E is defined as the energy before scattering at some depth x in the sample, and E may be written as

$$E(x) = E_0 - \int (dE/dx)dx \ . \tag{4}$$

The term dE/dx is a function of E rather than x, so the integral cannot be solved as written. The problem is resolved by writing x as a function of E.[6]

$$dx = (dx/dE)dE = (dE/dx)^{-1}dE \ , \tag{5}$$

and so it follows that

$$x = -\int_{E_0}^{E} (dE/dx)^{-1}dE \ . \tag{6}$$

The relationship between the energy and depth along the inward path is

$$x/\cos\theta_1 = \int_{E_0}^{E} (dE/dx)^{-1}dE \ , \tag{7}$$

and for the outward path

$$x/\cos\theta_2 = -\int_{KE}^{E_1} (dE/dx)^{-1}dE \ . \tag{8}$$

The energies which are used as limits of integration in equations (7) and (8) are defined as the incident beam energy E_0, the energy at a depth before scattering E, the energy at a depth x after scattering KE, and detected energy E_1. These energies are shown in figure 6. For this present work, dE/dx was assumed to be constant along the inward and outward paths. Under this assumption, equations (7) and (8) are solved to give

$$E = E_0 - (x/\cos\theta_1)(dE/dx)\Big|_{in} \ ,$$

and (9)

$$E_1 = KE - (x/\cos\theta_2)(dE/dx)\Big|_{out} \ .$$

Eliminating E in these two expressions gives

$$KE_0 - E_1 = \left[(k/\cos\theta_1)(dE/dx)\Big|_{in} + (1/\cos\theta_2)(dE/dx)\Big|_{out} \right] x \ . \tag{10}$$

Let

$$KE_0 - E_1 \equiv \delta E \ , \tag{11}$$

and

$$[S] = \left[(K/\cos\theta_1)(dE/dx)\Big|_{in} + (1/\cos\theta_2)(dE/dx)\Big|_{out} \right] , \tag{12}$$

so that

$$\delta E = [S]x \ . \tag{13}$$

A quantity defined as the stopping cross section ε is related to the energy loss dE/dx by

$$\varepsilon = (1/N)(dE/dx) \ , \tag{14}$$

where $N \equiv$ number of target atoms per unit volume.[6]

Utilizing the stopping cross section, δE can be expressed as

$$\delta E = [\varepsilon]Nx \ , \tag{15}$$

where

$$[\varepsilon] = \left\{ (k/\cos\theta_1)(\varepsilon)_{in} + (1/\cos\theta_2)(\varepsilon)_{out} \right\} \ . \tag{16}$$

The term $[\varepsilon]$ is defined as the stopping cross section factor, and ε_{in} and ε_{out} are stopping cross sections for the inward and outward paths, respectively. Stopping cross sections can be calculated by several methods. For this work, a fifth-order polynomial fit to experimental data was used

$$\varepsilon = A_0 + A_1E + A_2E^2 + A_3E^3 + A_4E^4 + A_5E^5 \ . \tag{17}$$

The coefficients $A_0, \ldots, A_5$ are tabulated constants which are unique for each element.[6]

The calculations for this present work were carried out using the surface energy approximation (SEA). This approximation technique is used to analyze regions near the outer surface where dE/dx for an incident particle changes slowly. When the thickness x becomes appreciable (typically > 1,000 nm), the SEA becomes inaccurate, and other approximation techniques must be used. Other approximation techniques include the mean energy approximation (MEA) and the symmetrical mean energy approximation (SMEA).[6]

For an incident beam which strikes a sample at normal incidence, the number of particles A detected at some particular scattering angle is

$$A = \sigma\Omega QN\tau \ , \tag{18}$$

where

$\sigma \equiv$ Rutherford scattering cross section,

$\Omega \equiv$ detector solid angle (str),

$Q \equiv$ number of incident particles,

$N \equiv$ number of target atoms per unit volume,

$\tau \equiv$ target thickness.

Considering surface and near-surface regions of the target, equation (18) can be expressed as[6]

$$H_0 = \sigma(E_0)\Omega Q N \tau_0 . \tag{19}$$

In equation (19), H_0 is the yield in one channel of the RBS spectrum, and τ_0 is a corresponding layer thickness in the sample such that scattering from anywhere within τ_0 produces counts in the channel corresponding to H_0. For the case of an incident beam impinging the target at some angle other than 0°, equation (19) is rewritten as

$$H_0 = \sigma E_0 \Omega Q N \tau_0 / \cos \theta_1 . \tag{20}$$

The thickness per channel τ_0 is defined by the energy width per channel $\boldsymbol{E}$ as[6]

$$\boldsymbol{E} = [\varepsilon_0] N \tau_0 . \tag{21}$$

Using equation (21), equation (20) can be expressed as

$$H_0 = \sigma(E_0)\Omega Q \boldsymbol{E} / [\varepsilon_0] . \tag{22}$$

The theory thus far has been developed for a sample composed of a single element. For compound samples, energy loss calculations are performed using Bragg's rule, which states that the total stopping cross section in a compound composed of various atomic species is the sum of the stopping cross sections of the constituent elements weighted proportionally by their abundance in the compound.[6] For example, suppose a compound AB has a composition $mA+nB$, then the stopping cross section for the compound can be expressed as

$$\varepsilon^{AB} = m\varepsilon^{A} + n\varepsilon^{B} . \tag{23}$$

The ratio (m/n) is the ratio of element A to element B. When this ratio is unknown, the method used to determine m/n involves comparing peak signal heights (fig. 7). These heights are

$H_A^A \equiv$ height for element A in layer composed of A,

$H_A^{AB} \equiv$ height for element A in compound AB,

$H_B^{AB} \equiv$ height of element B in compound AB,

$H_B^B \equiv$ height for element B in layer composed of B.

The following notation is used in this present work. Superscripts refer to the medium which the incident alpha particle traverses, and subscripts refer to the element involved in a scattering event.

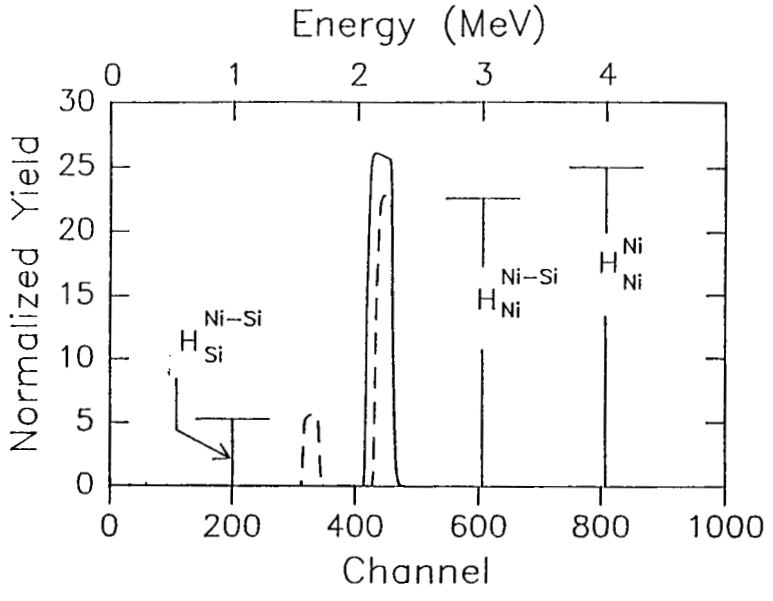

Figure 7. Simulated RBS spectra for thin layers of Ni (solid) and the compound Ni_2-Si (dashed).[7] (Both layer thicknesses are 200 nm and the Ni atomic densities are 9.14×10^{22} and 5.96×10^{22} atoms/cm^3 for the pure and compound samples, respectively.)

For a beam incident along the target normal, the height H_A^A is expressed as

$$H_A^A = \sigma_A(E)\Omega Q E/[\varepsilon]_A^A \ , \tag{24}$$

whereas the height

$$H_A^{AB} = \sigma_A(E)\Omega Q m E/[\varepsilon]_A^{AB} \ . \tag{25}$$

The value m appears in equation (25) as the result of the following density considerations.

Equation (19) can be rewritten for the height of element A in the compound A_mB_n as

$$H_A^{AB} = \sigma_A(E_0)\Omega Q N_A^{AB}\tau_A \ . \tag{26}$$

In equation (26), N_A^{AB} is the atomic number density for element A in the compound A_mB_n. N^{AB} is the molecular number density for the compound so that $N_A^{AB} = mN^{AB}$. Equation (21) is rewritten for the compound AB as

$$E = [\varepsilon]_A^{AB} N^{AB} \tau_A \ , \tag{27}$$

and substituted into equation (26). The result is equation (25).

The stopping cross section factor in equation (25) assumes Bragg's rule and is expressed as

$$[\varepsilon]_A^{AB} = m[\varepsilon]_A^A + n[\varepsilon]_A^B \ . \tag{28}$$

To determine the ratio of A to B in compound AB, the ratio of H_A^{AB} to H_A^A is written as

$$H_A^A / H_A^{AB} = \left\{ \sigma_A \Omega Q E [\varepsilon]_A^{AB} \right\} / \left\{ \sigma_A \Omega Q m E [\varepsilon]_A^A \right\} \ . \tag{29}$$

Provided that the detector solid angle, number of incident particles, and the energy per channel remain constant throughout the experiment, σ_A, Ω, Q, and E will cancel leaving

$$H_A^A / H_A^{AB} = [\varepsilon]_A^{AB} / m[\varepsilon]_A^A \ . \tag{30}$$

Using equation (28) to express the stopping cross section factor $[\varepsilon]_A^{AB}$, equation (30) is

$$H_A^A / H_A^{AB} = \left\{ m[\varepsilon]_A^A + n[\varepsilon]_A^B \right\} / \left\{ m[\varepsilon]_A^A \right\} \ , \tag{31}$$

and[7]

$$H_A^A / H_A^{AB} = 1 + (n/m) \left\{ [\varepsilon]_A^B / [\varepsilon]_A^A \right\} \ . \tag{32}$$

The ratio (n/m) in equation (32) is the ratio of element B to element A in the compound AB.

A second method for finding the ratio of A to B is the comparison of the signal height of the element A in AB to the signal height of element B in AB. Equation (29) is used to represent the height of element A and

$$H_B^{AB} = \sigma_B(E) \Omega Q n E / [\varepsilon]_B^{AB} \ , \tag{33}$$

is used to represent the height of element B in AB. The ratio of these peak heights is given by

$$H_A^{AB} / H_B^{AB} = \left\{ \sigma_A(E) m [\varepsilon]_B^{AB} \right\} / \left\{ \sigma_B(E) n [\varepsilon]_A^{AB} \right\} \ , \tag{34}$$

and the ratio (m/n) is the ratio of element A to element B in compound AB. For most elements A and B, the ratio $[\varepsilon]_B^{AB} / [\varepsilon]_A^{AB}$ is approximately equal to one.[6]

The thickness for a single element layer can be calculated by solving equation (21) for τ as

$$\tau = E / [\varepsilon] N \ . \tag{35}$$

If the layer is a compound, the equation is expressed as

$$\tau_A = E / [\varepsilon]_A^{AB} N^{AB} \quad \text{or} \quad \tau_B = E / [\varepsilon]_B^{AB} N^{AB} \ . \tag{36}$$

The variable τ_A represents the characteristic thickness per channel in a peak corresponding to element A in the compound AB. The width of this peak in channel numbers multiplied by τ_A yields the layer thickness for the compound AB.

CONCLUSIONS

This investigation did not prove conclusively that radiation enhanced diffusion is prevalent in anodic coatings of Al and Ta. This investigation did show the usefulness of RBS in understanding the phenomena present at a subsurface interface. The remainder of the conclusion section will concentrate on the data obtained from this investigation and provide an explanation for observed differences.

Figure 8 shows the anodized Al sample which was exposed to 2.0 MeV protons at a fluence of 1×10^{15} p+/cm^2. The spectrum shows a shift in energy for the two spectra. This shift can be explained by observing the sample surface with a microscope. Figure 9 shows the sample surface of the anodized aluminum. Specifically, figure 9 shows the presence of a surface bubble which was caused by the anodizing process. The effect of this bubble on an RBS spectrum is to increase the path length of the incident alpha particle and thus the layer of material will appear to be thicker. This increase can be expressed as

$$L' = L_0/\cos\theta_1 \ . \tag{37}$$

Figure 10 is an RBS spectra showing a section of the sample surface in which the anodized layer has flaked off exposing the carbon substrate. The exposed carbon substrate produces the peak observed at channel 110 in figure 10.

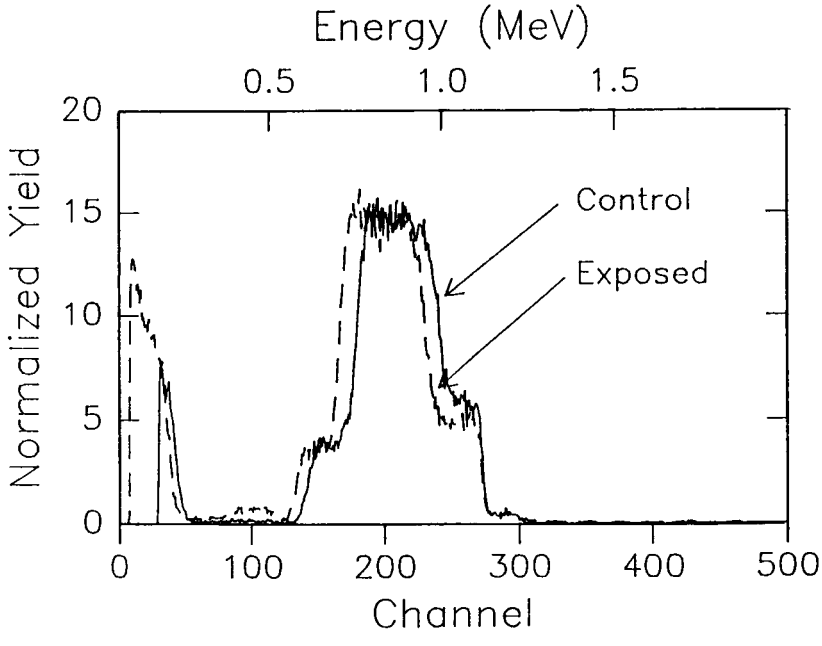

Figure 8. Anodized Al exposed to 2.0 MeV protons.

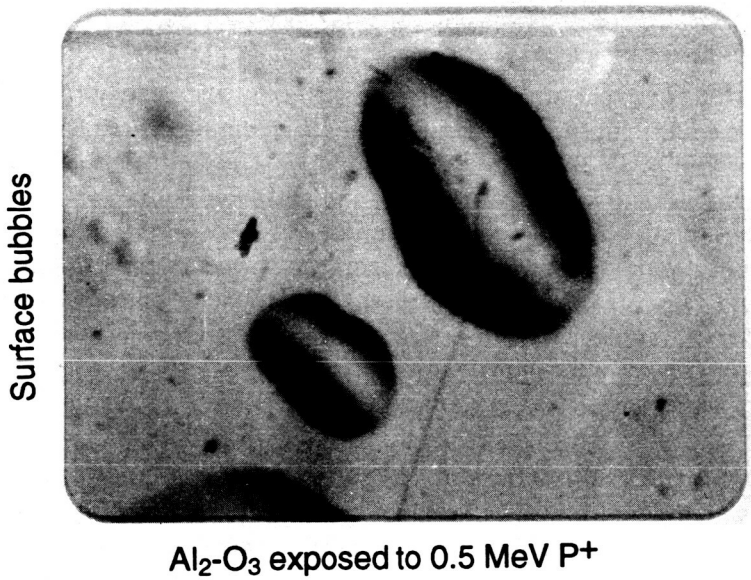

Figure 9. Surface of the anodized Al sample magnified × 40. (The bubbles shown will increase the path length of the incident alpha particle, used in RBS analysis.)

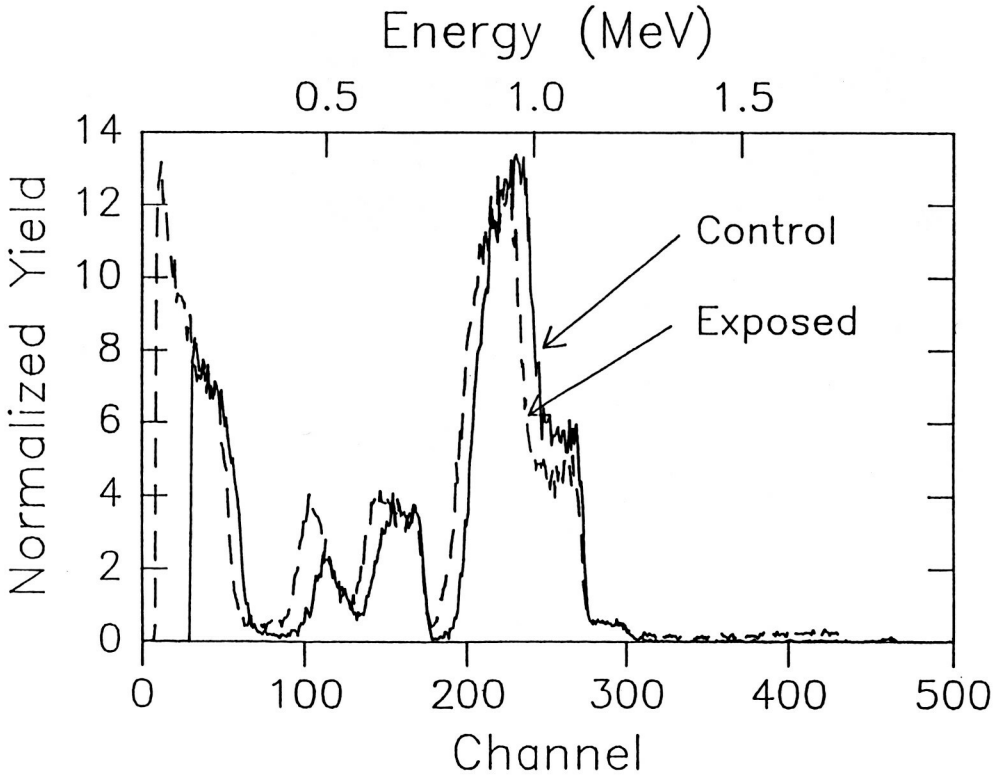

Figure 10. RBS spectra of a damaged anodized Al surface.

This spectrum indicates that the exposed carbon substrate was present before and after proton exposure. The peak height difference is due to the percentage increase in carbon surface area scanned by the RBS analysis beam. Figure 11 is a photograph of this section which has flaked off and exposed the carbon substrate. The anodized Ta samples showed no change to proton exposure when analyzed by RBS. Figure 12 shows the preexposure (control) and postexposure (exposed) RBS spectra. The control and exposed spectra are identical, indicating no measurable change in the sample. The realistic measure of a thermal control coating is the reflectance stability. The sample reflectivity was measured before and after exposure, and figure 13 shows the results for anodized Al. Close examination of this spectrum shows an increase in reflectance for the exposed samples in the region around 1,000 nm. This increase resembles a spike for both exposed samples. This increase is due to the percentage of exposed carbon on the surface of the sample. Recall from the RBS plots, the exposed carbon was present on the preexposure spectra. The decrease in overall reflectance is due to the decrease in percentage of Al_2-O_3 area scanned by the LPSR. Figure 13 does show some changes in the overall curve structure, which indicates a change in the surface properties.

These results were sufficient to initiate a larger investigation into the effects of charged particle radiation of chromic acid anodized Al which is baselined for use on Space Station *Freedom*. Figure 14 shows the effects of proton radiation on anodized Ta. As the spectrum indicates, Ta_2-O_5 is a poor reflector when compared to anodized Al. The reason for the decrease in reflectance between the exposed and control spectra is not positively known at this time. Since the RBS data indicated no change in the sample, speculation indicates the difference in reflectance is due, in part, to the increased percentage of exposed carbon surface area. Since Ta_2-O_5 has been shown to be a poor thermal control coating, this investigation simply noted that radiation exposure could have influenced the reflectance and presented the data showing the degradation.

Figure 11. A damaged bubble on the surface of the anodized Al sample. (The damaged region reveals the underlying diamond substrate.)

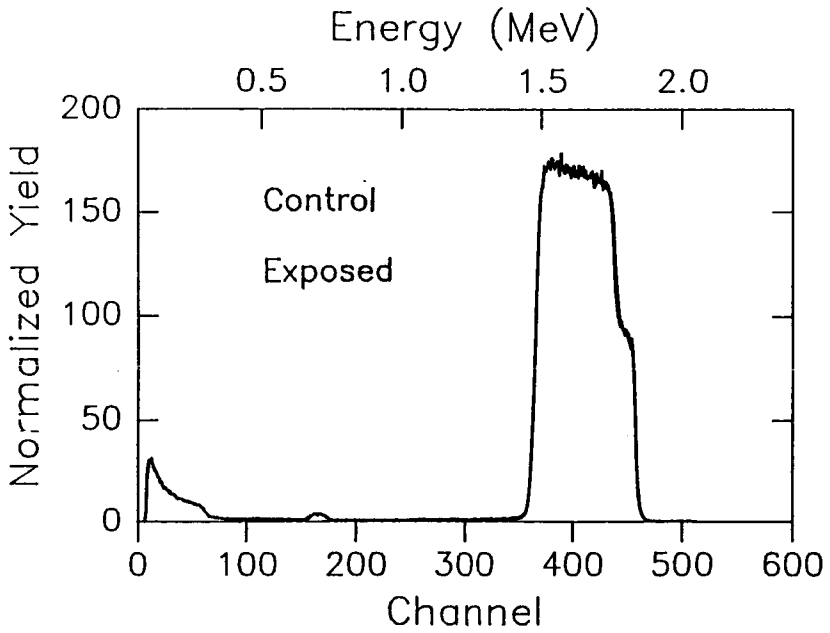

Figure 12. RBS spectra of anodized Ta.

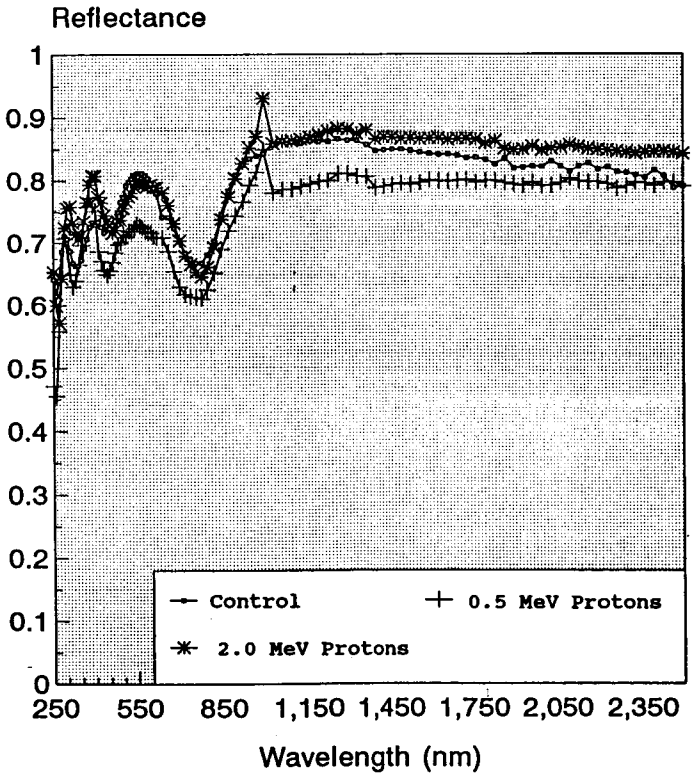

Figure 13. Comparison reflectance spectra of anodized Al before and after exposure to 0.5 and 2.0 MeV protons.

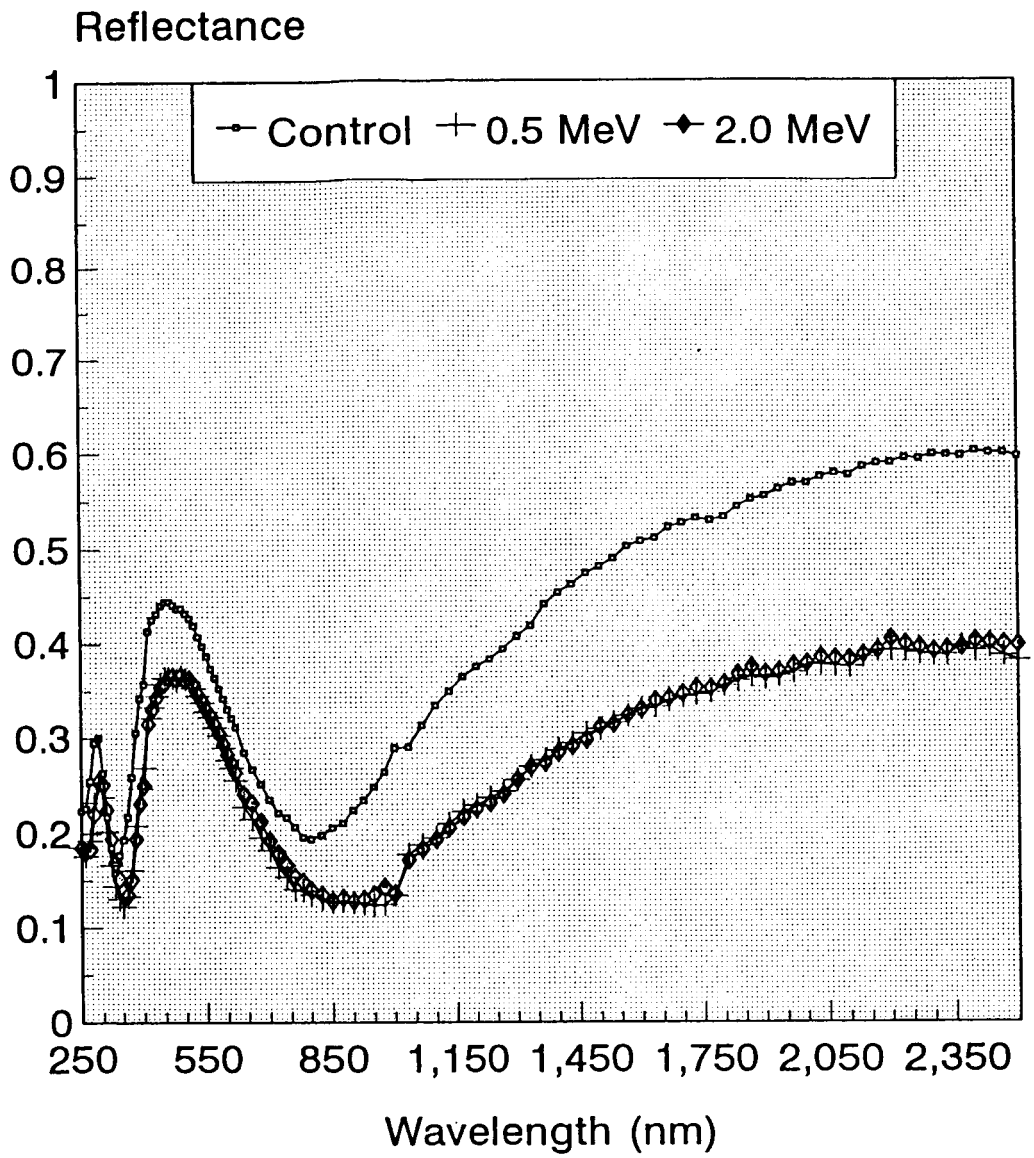

Figure 14. Comparison reflectance spectra of anodized Ta before and after exposure to 0.5 and 2.0 MeV protons.

REFERENCES

1. Levine, A.S.: "LDEF—69 Months in Space, First Post-Retrieval Symposium Parts 1, 2, and 3." NASA CP 3134, Kissimmee, FL, June 2–8, 1991.

2. "Space Radiation Protection." NASA SP-8054, June 1970.

3. Wilkes, D.R.: "Next Generation Optical Instruments and Space Experiment Based on the LDEF Thermal Control Surfaces Experiment (S0069)." Second LDEF Post-Retrieval Symposium, San Diego, CA, June 1–5, 1992.

4. Hitzig, J., et al.: Corrosion Science, vol. 24, 1984, pp. 11–12.

5. Pawel, R.E., et al.: J. Electrochemical Soc., vol. 114, 1959, p. 1223.

6. Chu, W.-K., Mayer, J.W., and Nicolet, M.-A.: "Backscattering Spectrometry." Academic Press, 1978.

7. Doolittle, L.: "RUMP Users Guide." Revision December 11, 1985.

APPROVAL

EVALUATION OF CHEMICAL CONVERSION MATERIAL (PROTECTIVE COATING) EXPOSED TO SPACE ENVIRONMENTAL CONDITIONS
CDDF Final Report (No. 90-07)

By D.L. Edwards

The information in this report has been reviewed for technical content. Review of any information concerning Department of Defense or nuclear energy activities or programs has been made by the MSFC Security Classification Officer. This report, in its entirety, has been determined to be unclassified.

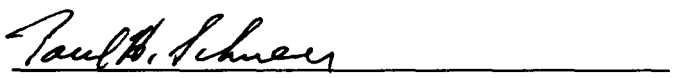

P.H. SCHUERER
Director, Materials and Processes Laboratory

☆ U.S. GOVERNMENT PRINTING OFFICE 1993—733-088/80091

REPORT DOCUMENTATION PAGE

Form Approved
OMB No. 0704-0188

1. AGENCY USE ONLY *(Leave blank)*	2. REPORT DATE	3. REPORT TYPE AND DATES COVERED
	July 1993	Technical Memorandum

4. TITLE AND SUBTITLE
Evaluation of Chemical Conversion Material (Protective Coating) Exposed to Space Environmental Conditions
CDDF Final Report (No. 90-07)

5. FUNDING NUMBERS

6. AUTHOR(S)
D.L. Edwards

7. PERFORMING ORGANIZATION NAME(S) AND ADDRESS(ES)
George C. Marshall Space Flight Center
Marshall Space Flight Center, Alabama 35812

8. PERFORMING ORGANIZATION REPORT NUMBER

9. SPONSORING / MONITORING AGENCY NAME(S) AND ADDRESS(ES)
National Aeronautics and Space Administration
Washington, DC 20546

10. SPONSORING / MONITORING AGENCY REPORT NUMBER
NASA TM - 108416

11. SUPPLEMENTARY NOTES
Prepared by Materials and Processes Laboratory, Science and Engineering Directorate.

12a. DISTRIBUTION / AVAILABILITY STATEMENT
Unclassified—Unlimited

12b. DISTRIBUTION CODE

13. ABSTRACT *(Maximum 200 words)*

This report focuses on the development of an operational Rutherford backscattering spectrometry (RBS) system and shows the application of such a system on a space environmental test.

Thin films of aluminum and tantalum were deposited on diamond substrates. These films were anodized and preexposure characterization spectra obtained using RBS and total hemispherical reflectance. The samples were exposed to energetic protons then postexposure characterization spectra was obtained using the same techniques.

Conclusions based on the comparison of preexposure and postexposure spectra are presented. RBS comparison spectra show no change in the metal/metal oxide interface, while the comparison reflectance data indicate change. Explanations for this reflectance change are presented in this report.

14. SUBJECT TERMS	15. NUMBER OF PAGES
Rutherford backscattering spectrometry (RBS), protons, space environmental effects, reflectance, anodize aluminum	22
	16. PRICE CODE NTIS

17. SECURITY CLASSIFICATION OF REPORT	18. SECURITY CLASSIFICATION OF THIS PAGE	19. SECURITY CLASSIFICATION OF ABSTRACT	20. LIMITATION OF ABSTRACT
Unclassified	Unclassified	Unclassified	Unlimited